

Supplementary Information

Zinc pyrithione is a potent inhibitor of PL^{Pro} and cathepsin L enzymes with *ex vivo* inhibition of SARS-CoV-2 entry and replication

Jerneja Kladnik¹, Ana Dolinar¹, Jakob Kljun¹, David Perea², Judith Grau-Expósito², Meritxell Genescà², Marko Novinec¹, Maria J. Buzon^{2,*}, Iztok Turel^{1,*}

¹ Faculty of Chemistry and Chemical Technology, University of Ljubljana, Večna pot 113, SI-1000 Ljubljana, Slovenia

² Infectious Diseases Department, Vall d'Hebron Research Institute (VHIR), Hospital Universitari Vall d'Hebron, Universitat Autònoma de Barcelona, VHIR Task Force COVID-19, Barcelona, Spain

* Corresponding authors: mariajose.buzon@vhir.org, iztok.turel@fkkt.uni-lj.si

Table of Contents

1. General information	2
2. Characterization of zinc complexes	3
3. Crystal structures	5
4. NMR spectra	8
5. UV-vis and NMR stability	16
6. Enzyme assays	21
7. Prediction data for the key parameters in drug design	24
8. References	25

1. General information

Ligand pyrithione **a**, starting materials and other reagents as well as solvents for the synthesis of ligands **b–h**, complexes **1a–h** and **2a**, were purchased from commercial suppliers (Fluorochem, Alfa Aesar, Riedel-de-Haën, Merck) and used as received without further purification.

The progress of the reaction was monitored by thin layer chromatography using pre-coated TLC sheets ALUGRAM® SIL G/UV254 (Macherey–Nagel) visualised with UV lamp (254 nm). The column chromatography of the ligands was carried out on Merck silica gel 60 (35–70 mm). ¹H NMR spectra for compound characterization were acquired on Bruker Avance III 500 spectrometer at room temperature at 500 MHz. ¹H NMR stability spectra were obtained on NMR Bruker AvanceNeo 600 MHz spectrometer at room temperature at 600 MHz. All chemical shifts (δ) in the spectra of the complexes are referenced to the residual peaks of deuterated solvent (CD₃)₂SO, CDCl₃ and D₂O at 2.50 (referenced to the central line of a quintet), 7.26 and 4.79 ppm, respectively and are reported in ppm. Coupling constants (*J*) are reported in Hz. Spectra were processed in MestReNova 11.0.4. The multiplicity of the signals is abbreviated as s – singlet, d – doublet, t – triplet and m – multiplet. IR spectra were obtained on a Bruker FTIR Alpha Platinum ATR spectrometer. High resolution mass spectrometry was performed on an Agilent 6224 Accurate Mass TOF LC/MS system. Elemental analysis (C, H, N) was carried out on a PerkinElmer 2400 II instrument. UV-vis spectroscopy was performed on a PerkinElmer LAMBDA 750 UV/Vis/near-IR spectrophotometer. For X-ray structural analysis, single crystals were surrounded with silicon grease, mounted onto the tip of glass fibres and transferred to the goniometer head in the liquid nitrogen cryostream (150(2) K). Data were collected on a SuperNova diffractometer equipped with Atlas detector using CrysAlis software with monochromated Mo K α (0.71073 Å).¹ The initial structural models were obtained via direct methods using the Olex2 graphical user interface² implemented in SHELXT. A full-matrix least-squares refinement on *F*² magnitudes with anisotropic displacement parameters for all non-hydrogen atoms using Olex2 or SHELXL-2018/3 was employed.^{2,3} All non-hydrogen atoms were refined anisotropically, while the hydrogen atoms were placed at calculated positions and further treated as riding on their parent atoms. Figures depicting the structures were prepared with Mercury.⁴ The crystal structures have been submitted to the CCDC and have been allocated the deposition numbers 2143703-2143706. These data are provided free of charge by The Cambridge Crystallographic Data Centre.⁵

Synthetic fluorogenic substrates benzyloxycarbonyl-Leu-Arg-7-amino-4-methylcoumarin (Z-LR-AMC; Cat. No. 4034611) and benzyloxycarbonyl-Arg-Leu-Arg-Gly-Gly-7-amino-4-methylcoumarin (Z-RLRGG-AMC; Cat. No. 4027158) were purchased from Bachem. Ni-affinity column HisTrap was purchased from GE Healthcare.

OD₆₀₀ measurements were obtained with Varian Cary 50 Bio spectrophotometer (Agilent). Protein elution was performed on ÄKTA FPLC system (GE Healthcare). Enzymatic kinetic measurements were performed on a PerkinElmer LS55 fluorescence spectrometer with PTP-1 Fluorescence Peltier System and Peltier Controlled Fluid Circulator (PCB1500).

2. Characterization of zinc complexes

[Zn(II)(1-hydroxypyridine-2(1*H*)-thionato)₂] (**1a**).

Yield: 89%. ¹H NMR (500 MHz, (CD₃)₂SO): δ = 8.43 (dd, 2H, *J* = 6.6, 1.2 Hz, Ar-*H* a), 7.61 (dd, 2H, *J* = 8.2, 1.8 Hz, Ar-*H* a), 7.28–7.22 (m, 2H, Ar-*H* a), 7.01 (td, 2H, *J* = 7.0, 1.8 Hz, Ar-*H* a) ppm. ESI-HRMS (CH₃CN): *m/z* calcd for [C₁₀H₉N₂O₂S₂Zn]⁺: 316.9391; found: 316.9391. Elemental analysis calcd (%) for C₁₀H₈N₂O₂S₂Zn: C, 37.81; H, 2.54; N, 8.82; found: C, 37.59; H, 2.50; N, 8.59. IR selected bands (ATR): $\tilde{\nu}$ = 3102, 1457, 1199, 1147, 1087, 821, 762, 703, 582, 564 cm⁻¹.

[Zn(II)(1-hydroxy-3-methylpyridine-2(1*H*)-thionato)₂] (**1b**).

Yield: 87%. ¹H NMR (500 MHz, CDCl₃): δ = 8.26 (dd, 2H, *J* = 6.6, 0.6 Hz, Ar-*H* b), 7.24–7.20 (m, 2H, Ar-*H* b), 6.84 (t, 2H, *J* = 7.0 Hz, Ar-*H* b), 2.52 (s, 6H, Ar-CH₃ b) ppm. ESI-HRMS (CH₃CN): *m/z* calcd for [C₁₂H₁₃N₂O₂S₂Zn]⁺: 344.9704; found: 344.9702. Elemental analysis calcd (%) for C₁₂H₁₂N₂O₂S₂Zn: C, 41.69; H, 3.50; N, 8.10; found: C, 41.34; H, 3.40; N, 8.00. IR selected bands (ATR): $\tilde{\nu}$ = 3073, 1403, 1206, 1146, 1134, 782, 702, 630, 565 cm⁻¹.

[Zn(II)(1-hydroxy-4-methylpyridine-2(1*H*)-thionato)₂] (**1c**).

Yield: 50%. ¹H NMR (500 MHz, CDCl₃): δ = 8.16 (d, 2H, *J* = 6.8 Hz, Ar-*H* c), 7.53 (dd, 2H, *J* = 1.6, 0.6 Hz, Ar-*H* c), 6.72 (dd, 2H, *J* = 6.8, 2.4 Hz, Ar-*H* c), 2.30 (s, 6H, Ar-CH₃ c) ppm. ESI-HRMS (CH₃CN): *m/z* calcd for [C₁₂H₁₃N₂O₂S₂Zn]⁺: 344.9704; found: 344.9701. Elemental analysis calcd (%) for C₁₂H₁₂N₂O₂S₂Zn: C, 41.69; H, 3.50; N, 8.10; found: C, 41.53; H, 3.50; N, 7.97. IR selected bands (ATR): $\tilde{\nu}$ = 3072, 1614, 1469, 1197, 1138, 1085, 809, 780, 602, 488 cm⁻¹.

[Zn(II)(1-hydroxy-5-methylpyridine-2(1*H*)-thionato)₂] (**1d**).

Yield: 72%. ¹H NMR (500 MHz, CDCl₃): δ = 8.14 (s, 2H, Ar-*H* d), 7.61 (d, 2H, *J* = 8.5 Hz, Ar-*H* d), 7.07 (dd, 2H, *J* = 8.5, 1.4 Hz, Ar-*H* d), 2.26 (s, 6H, Ar-CH₃ d) ppm. ESI-HRMS (CH₃CN): *m/z* calcd for [C₁₂H₁₃N₂O₂S₂Zn]⁺: 344.9704; found: 344.9705. Elemental analysis calcd (%) for C₁₂H₁₂N₂O₂S₂Zn: C, 41.69; H, 3.50; N, 8.10; found: C, 41.39; H, 3.38; N, 8.08. IR selected bands (ATR): $\tilde{\nu}$ = 3056, 1474, 1372, 1149, 1090, 810, 739, 664, 592, 548 cm⁻¹.

[Zn(II)(1-hydroxy-6-methylpyridine-2(1*H*)-thionato)₂] (**1e**).

Yield: 54%. ¹H NMR (500 MHz, CDCl₃): δ = 7.63 (dd, 2H, *J* = 8.3, 1.5 Hz, Ar-*H* e), 7.10 (t, 2H, *J* = 7.7 Hz, Ar-*H* e), 6.85 (dd, 2H, *J* = 7.7, 1.5 Hz, Ar-*H* e), 2.61 (s, 6H, Ar-CH₃ e) ppm. ESI-HRMS (CH₃CN): *m/z* calcd for [C₁₂H₁₃N₂O₂S₂Zn]⁺: 344.9704; found: 344.9702. Elemental analysis calcd (%) for C₁₂H₁₂N₂O₂S₂Zn: C, 41.69; H, 3.50; N, 8.10; found: C, 41.26; H, 3.39; N, 7.97. IR selected bands (ATR): $\tilde{\nu}$ = 3072, 1557, 1461, 1373, 1200, 1184, 889, 770, 646, 411 cm⁻¹.

[Zn(II)(2-hydroxyisoquinoline-1(2*H*)-thione)₂] (**1f**).

Yield: 93 %. ¹H NMR (500 MHz, CDCl₃): δ = 8.77–8.72 (m, 2H, Ar-*H* f), 8.22 (d, 2H, *J* = 7.2 Hz, Ar-*H* f), 7.78–7.73 (m, 2H, Ar-*H* f), 7.72–7.66 (m, 4H, Ar-*H* f), 7.30 (d, 2H, *J* = 7.2 Hz, Ar-*H* f) ppm. ESI-HRMS (CH₃CN): *m/z* calcd for [C₁₈H₁₃N₂O₂S₂Zn]⁺: 416.9704; found: 416.9708. Elemental analysis calcd (%) for C₁₈H₁₂N₂O₂S₂Zn: C, 51.75; H, 2.90; N, 6.71; found: C, 51.48; H, 2.67; N, 6.60. IR selected bands (ATR): $\tilde{\nu}$ = 3088, 2970, 1547, 1334, 1306, 1199, 948, 789, 762, 746, 667 cm⁻¹.

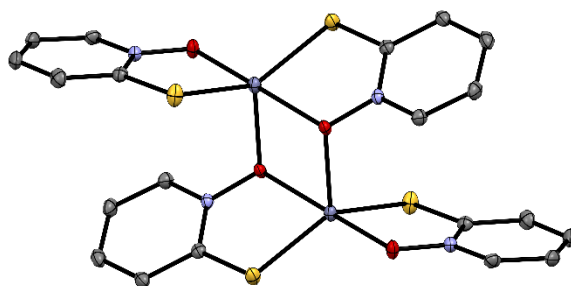
[Zn(II)(1-hydroxyquinoline-2(1*H*)-thione)₂] (**1g**).

Yield: 70 %. ¹H NMR (500 MHz, CDCl₃): δ = 8.64 (d, 2H, *J* = 8.8 Hz, Ar-*H* g), 7.79–7.70 (m, 6H, Ar-*H* g), 7.66 (d, 2H, *J* = 8.8 Hz, Ar-*H* g), 7.53–7.48 (m, 2H, Ar-*H* g) ppm. ESI-HRMS (CH₃CN): *m/z* calcd for [C₁₈H₁₃N₂O₂S₂Zn]⁺: 416.9704; found: 416.9704. Elemental analysis calcd (%) for C₁₈H₁₂N₂O₂S₂Zn: C, 51.75; H, 2.90; N, 6.71; found: C, 51.87; H, 2.61; N, 6.72. IR selected bands (ATR): $\tilde{\nu}$ = 2970, 1738, 1600, 1561, 1306, 902, 808, 757, 654, 512 cm⁻¹.

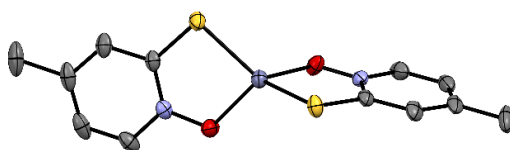
[Zn(II)(1-hydroxy-3-methoxypyridine-2(1*H*)-thionato)₂] (**1h**).

Yield: 57%. ¹H NMR (500 MHz, CDCl₃): δ = 8.08 (dd, 2H, *J* = 6.5, 1.0 Hz, Ar-*H* h), 6.90–6.80 (m, 4H, Ar-*H* h), 3.98 (s, 6H, Ar-OCH₃ h) ppm. ESI-HRMS (CH₃CN): *m/z* calcd for [C₁₂H₁₃N₂O₄S₂Zn]⁺: 376.9603; found: 376.9598. Elemental analysis calcd (%) for C₁₂H₁₂N₂O₄S₂Zn: C, 38.16; H, 3.20; N, 7.42; found: C, 37.97; H, 3.00; N, 7.47. IR selected bands (ATR): $\tilde{\nu}$ = 3108, 1553, 1441, 1424, 1292, 1222, 1067, 762, 696, 669 cm⁻¹.

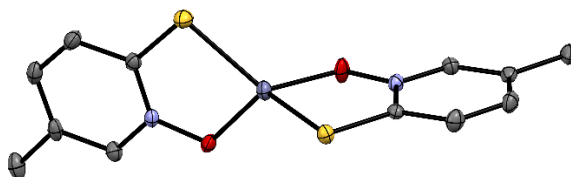
3. Crystal structures



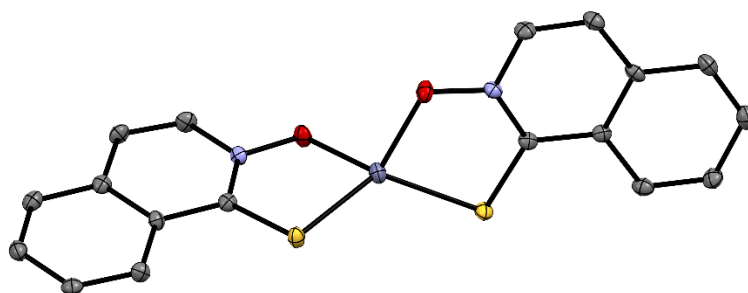
1a*



1c



1d



1f

Supplementary Figure 1: Crystal structure of complexes 1a, 1c, 1d and 1f. Ellipsoids are drawn at the 35% probability level. *As the structure report for **1a** dates back to 1977,⁶ we decided to re-measure data on a crystal sample of this compound to obtain high-quality data.

Supplementary Table 1: Crystallographic data for complexes 1a, 1c, 1d and 1d.

Compound	1a (moc470)	1c (mob156)	1d (mob128)	1f (moc457)
Empirical formula	C ₁₀ H ₈ N ₂ O ₂ S ₂ Zn	C ₁₂ H ₁₂ N ₂ O ₂ S ₂ Zn	C ₁₂ H ₁₂ N ₂ O ₂ S ₂ Zn	C ₁₈ H ₁₂ N ₂ O ₂ S ₂ Zn
Formula weight	317.67	345.73	345.769	417.79
Temperature/K	150(2)	150	150	150
Crystal system	monoclinic	trigonal	monoclinic	triclinic
Space group	P2 ₁ /c	R-3c	C2/c	P-1
a/Å	8.3347(4)	21.186(2)	27.7422(12)	7.0548(3)
b/Å	10.1317(4)	21.186(2)	7.2234(4)	7.0948(3)
c/Å	13.6447(6)	16.8962(9)	13.5512(6)	16.2539(9)
α/°	90	90	90	99.916(4)
β/°	96.748(4)	90	99.630(5)	95.707(4)
γ/°	90	120	90	98.714(4)
Volume/Å ³	1144.24(9)	6567.9(13)	2677.3(2)	785.53(7)
Z	4	18	8	2
ρ _{calc} [g/cm ³]	1.844	1.573	1.716	1.766
μ/mm ⁻¹	2.499	1.966	2.144	1.844
F(000)	640.0	3168.0	1413.1	424.0
Crystal size/mm ³	0.25 × 0.25 × 0.25	0.7 × 0.1 × 0.1	1.0 × 0.9 × 0.8	0.1 × 0.05 × 0.03
Radiation	Mo Kα (λ = 0.71073)	Mo Kα (λ = 0.71073)	Mo Kα (λ = 0.71073)	Mo Kα (λ = 0.71073)
2θ range for data collection/°	4.922 to 54.958	6.35 to 54.952	5.84 to 54.96	5.132 to 54.97
Index ranges	-10 ≤ h ≤ 10, -13 ≤ k ≤ 13, -16 ≤ l ≤ 17	-18 ≤ h ≤ 22, -27 ≤ k ≤ 27, -21 ≤ l ≤ 19	-38 ≤ h ≤ 25, -9 ≤ k ≤ 10, -17 ≤ l ≤ 18	-8 ≤ h ≤ 9, -9 ≤ k ≤ 9, -21 ≤ l ≤ 21
Reflections collected	11634	5691	8064	16062
Independent reflections	2609 [R _{int} = 0.0349, R _{sigma} = 0.0280]	1661 [R _{int} = 0.0245, R _{sigma} = 0.0207]	3075 [R _{int} = 0.0219, R _{sigma} = 0.0291]	3550 [R _{int} = 0.0513, R _{sigma} = 0.0428]
Data/restraints/parameters	2609/0/154	1661/0/88	3075/0/174	3550/0/226
Goodness-of-fit on F ²	1.055	1.251	1.050	1.137
Final R indexes [I ≥ 2σ(I)]	R ₁ = 0.0242, wR ₂ = 0.0534	R ₁ = 0.0446, wR ₂ = 0.0923	R ₁ = 0.0294, wR ₂ = 0.0738	R ₁ = 0.0695, wR ₂ = 0.1942
Final R indexes [all data]	R ₁ = 0.0302, wR ₂ = 0.0567	R ₁ = 0.0490, wR ₂ = 0.0941	R ₁ = 0.0350, wR ₂ = 0.0775	R ₁ = 0.0782, wR ₂ = 0.1990
Largest diff. peak/hole / eÅ ⁻³	0.33/-0.37	0.43/-0.34	0.47/-0.34	2.58/-0.76

Comment of crystal structure of **1f**: The checkcif report contains 2 B-type alerts due to residual peaks of electron density (Q1 2.58, Q2 2.56). These peaks cannot be refined by insertion of for example solvate water molecules. The absence of solvate water molecules is confirmed by CHN elemental analysis. The anomalies are attributed to lower quality of the single crystal. Despite that, all bond lengths and angles are within the value ranges typical for zinc complexes. At present this is the best data we were able to obtain.

Supplementary Table 2: Analysis of the available crystal structures of zinc-pyrrhione complexes.

			Zn1-O _{terminal}	Zn1-S	Zn1-O _{bridge}	O _{bridge} -Zn2	τ_5
OXPTZN ⁶ (Zn-pth complex, chloroform solvate)	1a	dimer	2.0502	2.3106 2.315	2.1847	2.0925	0.59
OXPTZND (Zn-pth complex)	1a	dimer	2.0494	2.3069 2.3075	2.1821	2.1215	0.52
MIKZEL	1b	dimer	2.049(3)	2.306(2) 2.295(2)	2.171(3)	2.127(4)	0.51
			Zn-O	Zn-S			τ_4/τ_4'
TETRAL ⁷ (Zn-(4Me-pth) complex, 1/6 ethanol solvate)	1c	monomer (symmetric)	1.968	2.275			0.78/0.74
Mob156 (Isostructural with TETRAL, EtOH atoms unassigned)	1c	monomer (symmetric)	1.973	2.270			0.78/0.74
Mob128 (Zn-(5Me-pth) complex)	1d	monomer	1.973(1) 1.968(1)	2.2859(7) 2.2729(8)			0.78/0.75
CAQCEC ⁸ (Zn-(6Me-pth) complex)	1e	monomer	1.983(2) 1.985(3)	2.2636(9) 2.2701(8)			0.76/0.70
Mob457 (Zn-(N-hydroxyisoquinoline-1-thione) complex)	1f	monomer	1.972(5) 1.965(4)	2.289(2) 2.286(1)			0.76/0.75

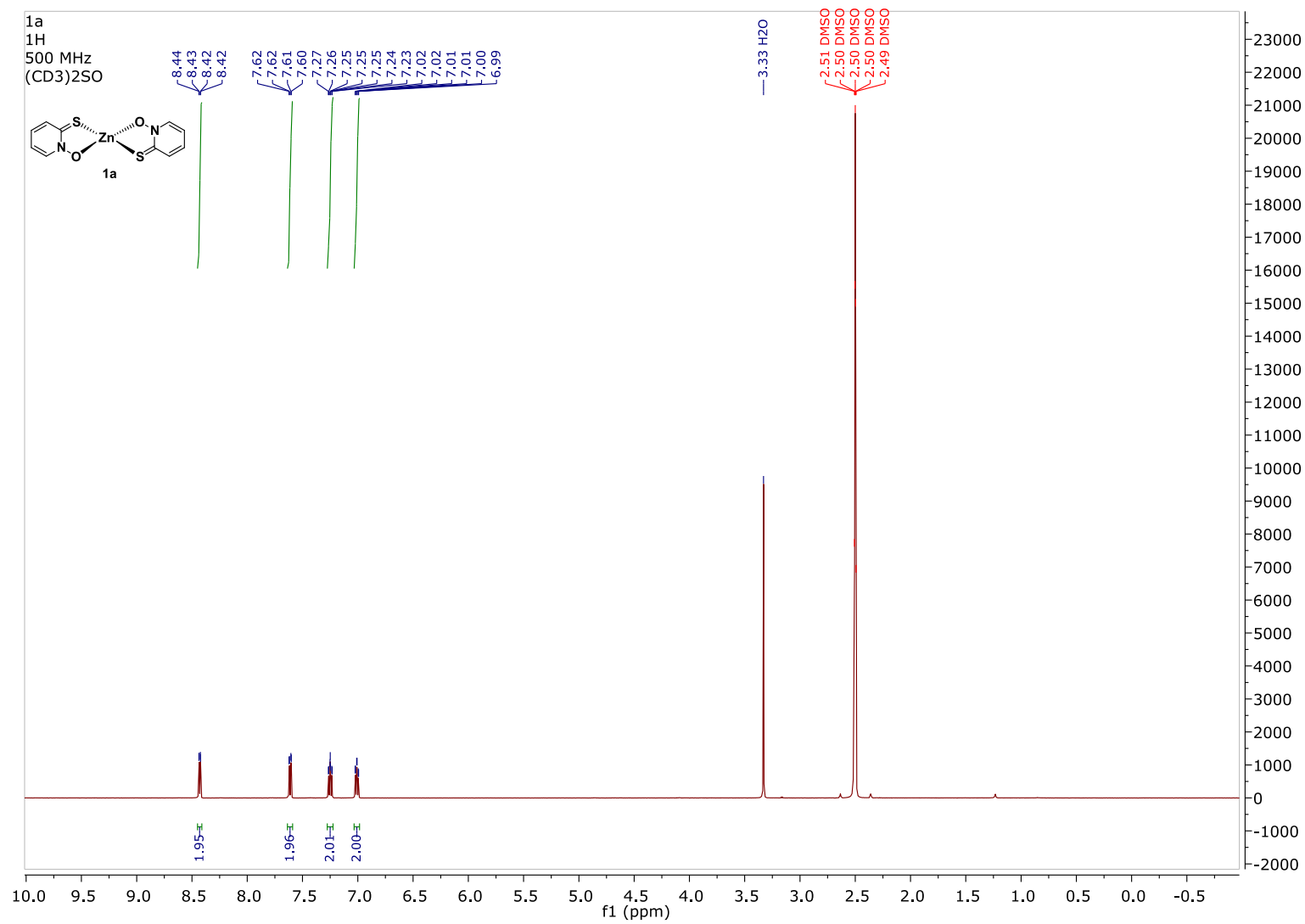
$\tau_5 = (\beta - \alpha)/(60^\circ)$. For square-pyramidal geometry, the τ_5 value is 0, for ideal trigonal-bipyramidal geometry, the value of τ_5 is 1. $\tau_4 = [360^\circ - (\alpha + \beta)]/(360^\circ - 2 \cdot \theta)$; $\tau_4' = [(\beta - \alpha)/(360^\circ - \theta)] + [(180^\circ - \beta)/(360^\circ - \theta)]$; α and β are the two greatest valence angles of coordination center, θ is tetrahedral angle 109.471° . For ideal square-planar geometry τ_4 and τ_4' values are 0, for ideal tetrahedral geometry τ_4 and τ_4' values are 1.

Reference for τ_4 : <https://pubs.rsc.org/en/content/articlelanding/2007/DT/B617136B>

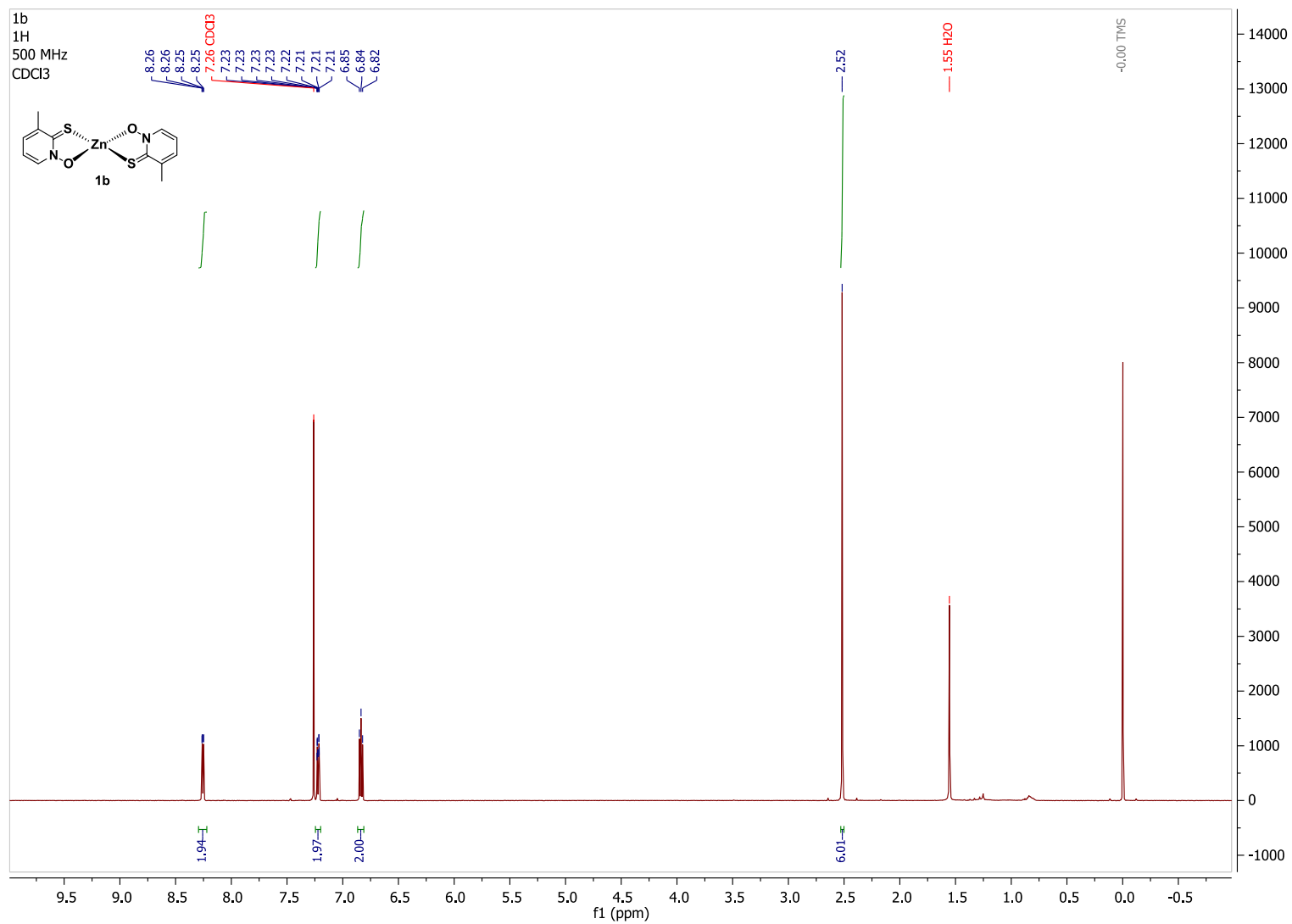
Reference for τ_4' : <https://www.sciencedirect.com/science/article/pii/S0277538715000625?via%3Dihub>

Reference for τ_5 : <https://pubs.rsc.org/en/content/articlelanding/1984/DT/DT9840001349>

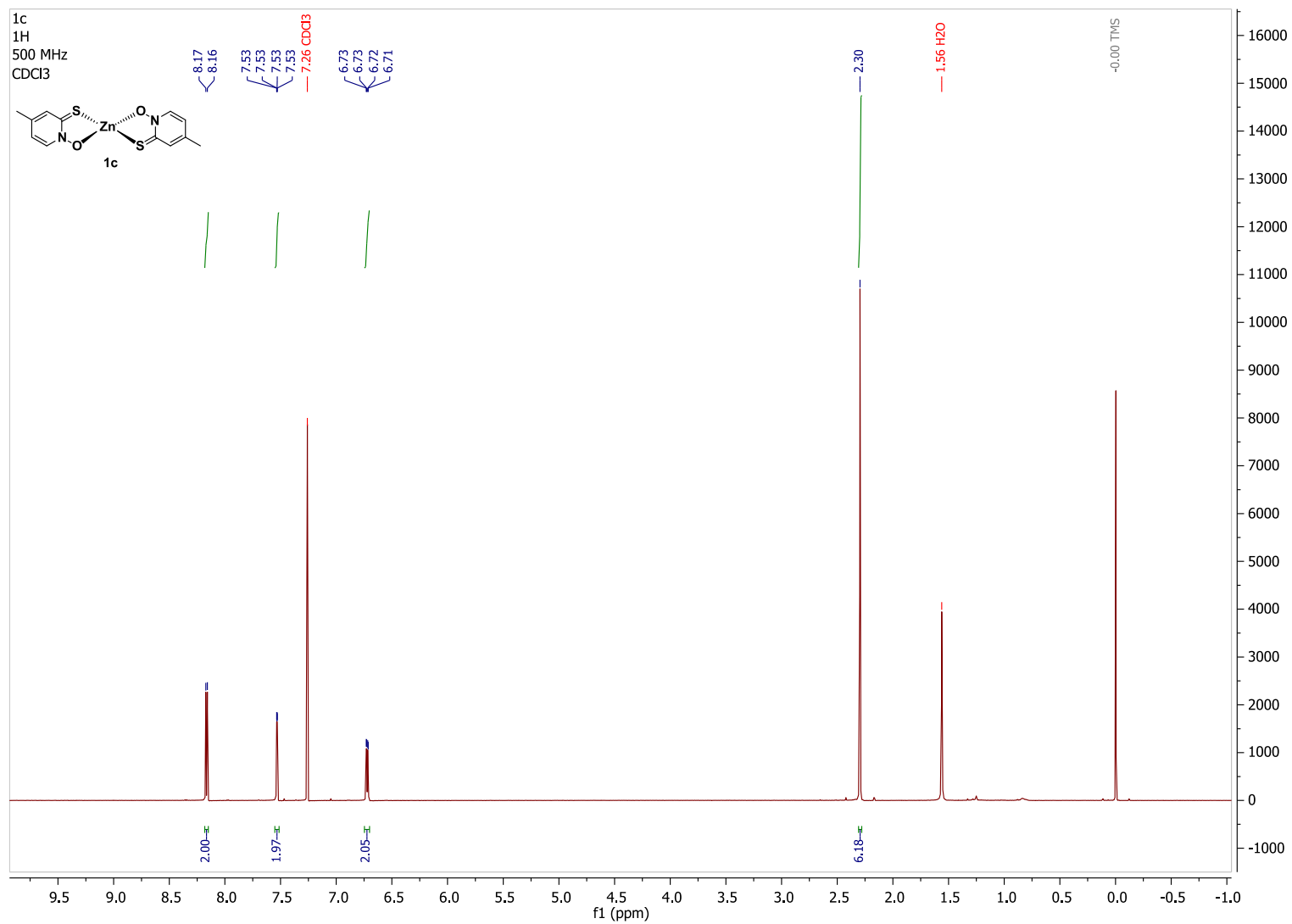
4. NMR spectra



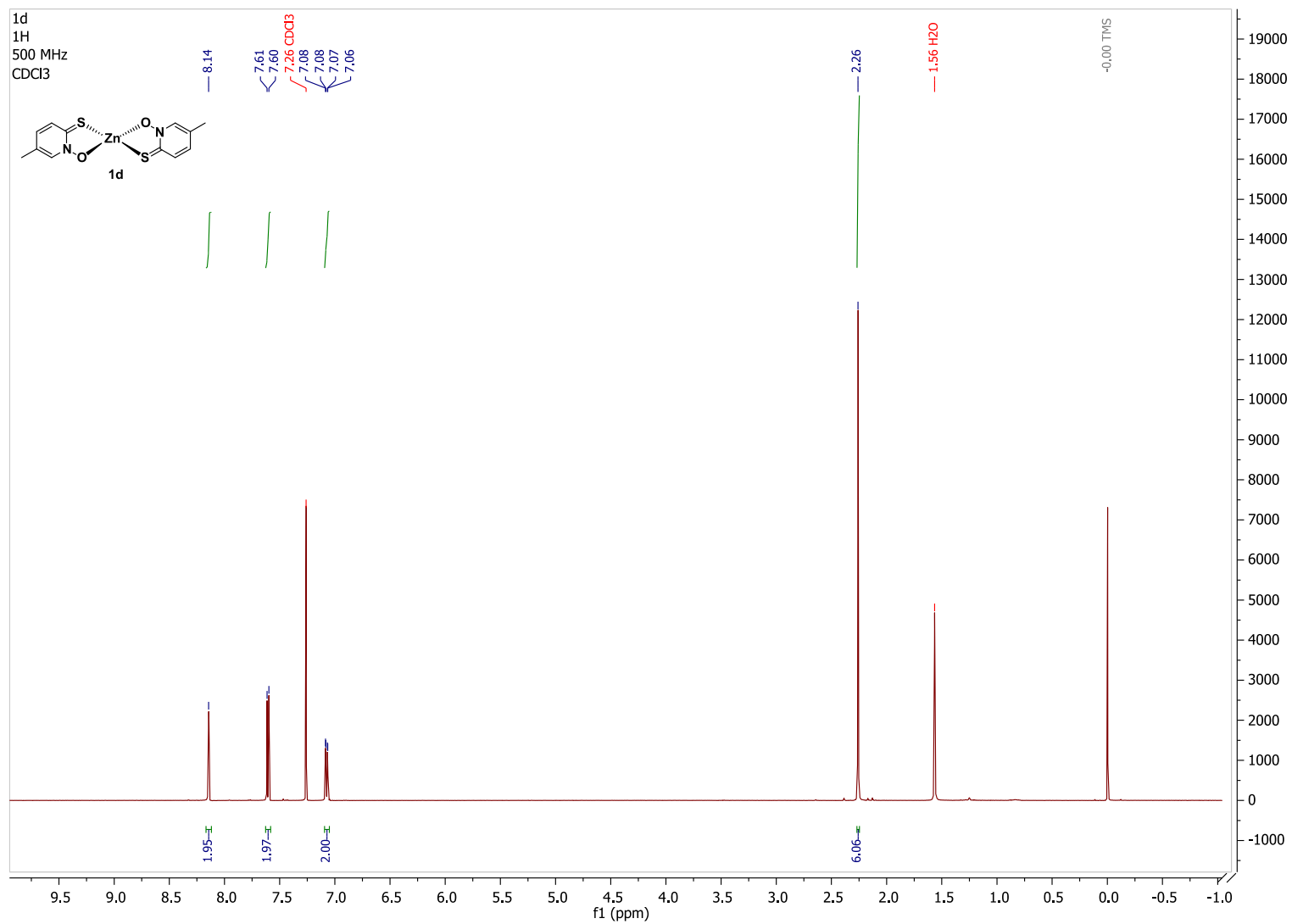
Supplementary Figure 2: ¹H NMR spectrum of 1a.



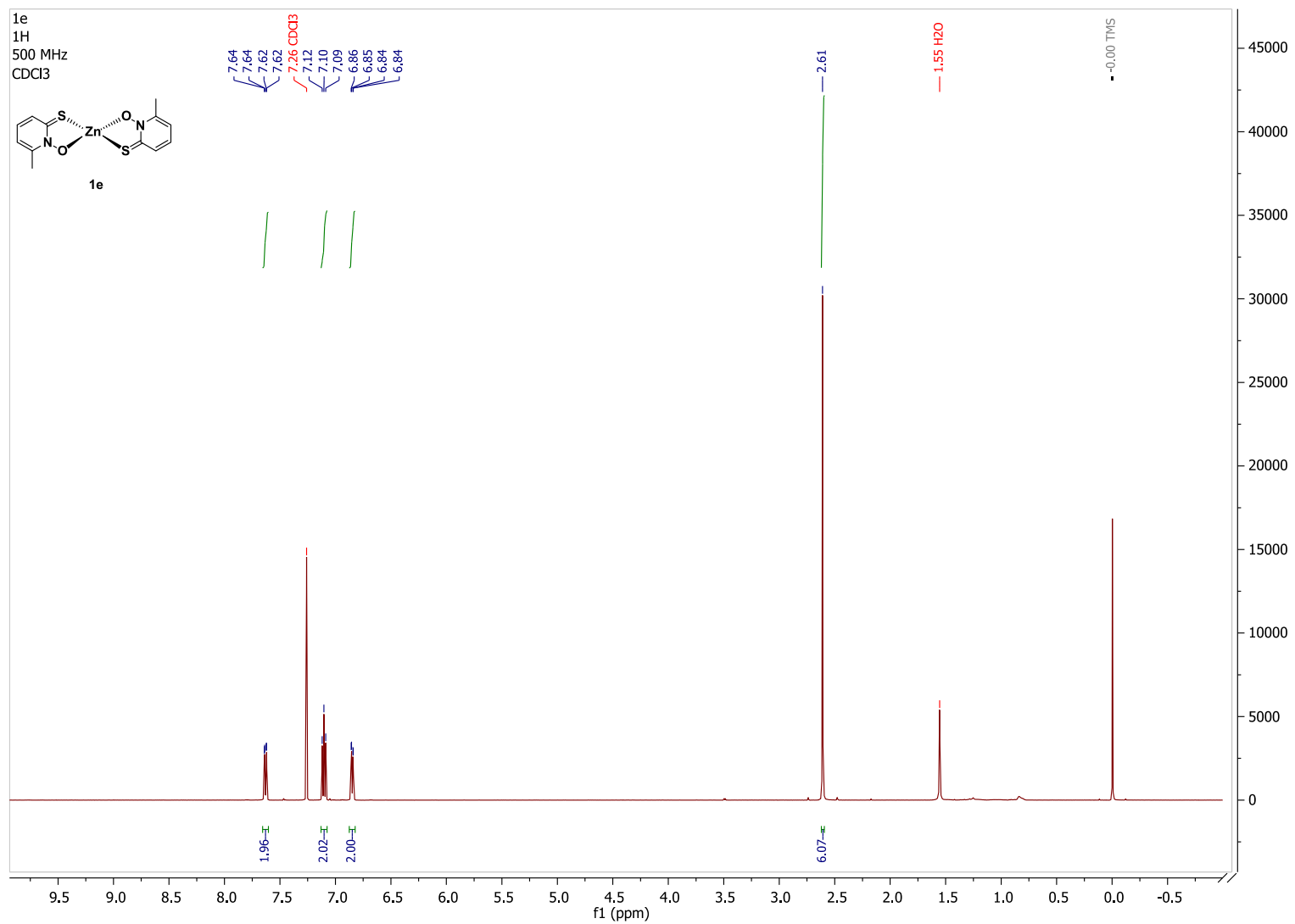
Supplementary Figure 3: ^1H NMR spectrum of 1b.



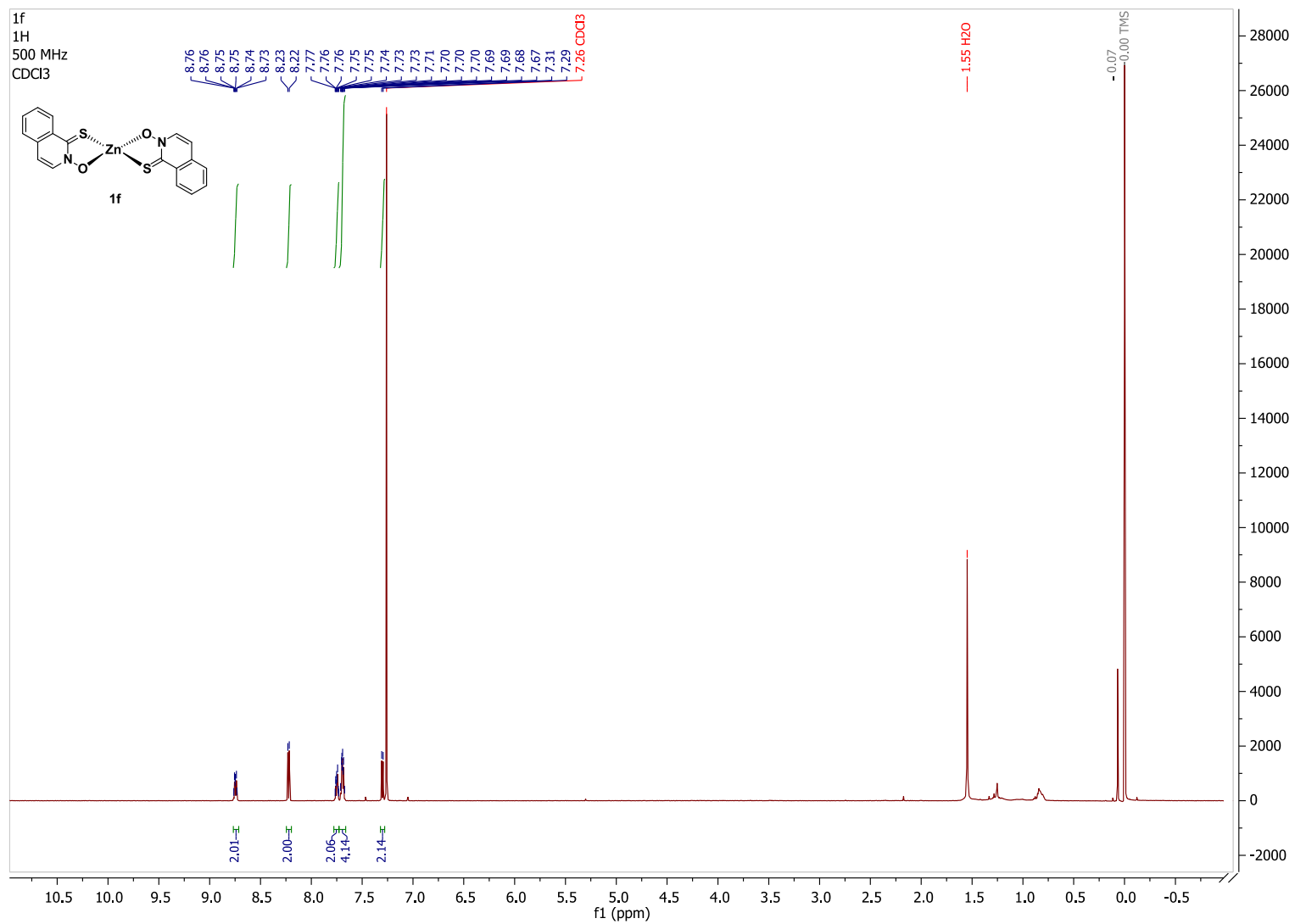
Supplementary Figure 4: ^1H NMR spectrum of 1c.



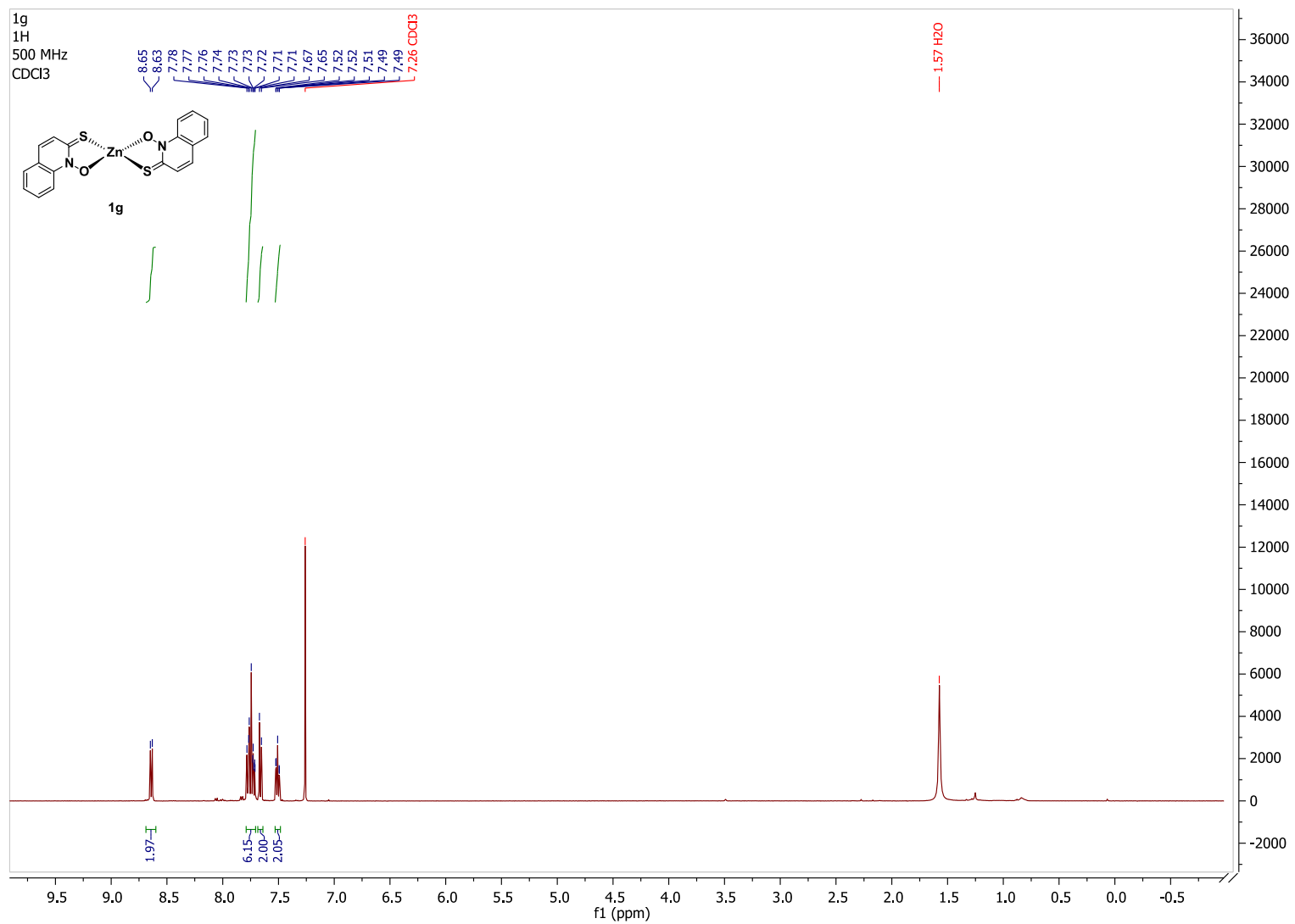
Supplementary Figure 5: ^1H NMR spectrum of 1d.



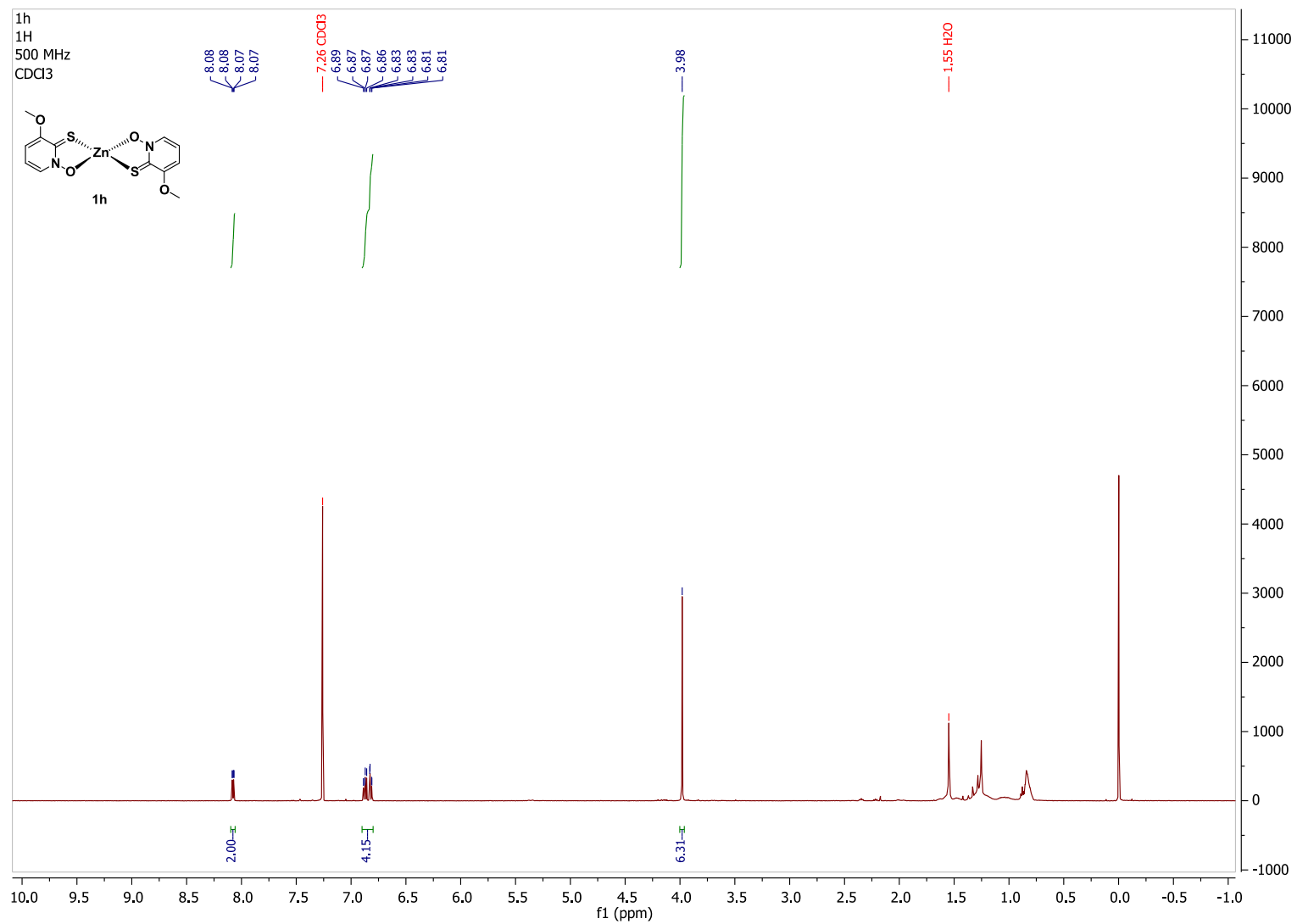
Supplementary Figure 6: ¹H NMR spectrum of 1e.



Supplementary Figure 7: ^1H NMR spectrum of 1f.

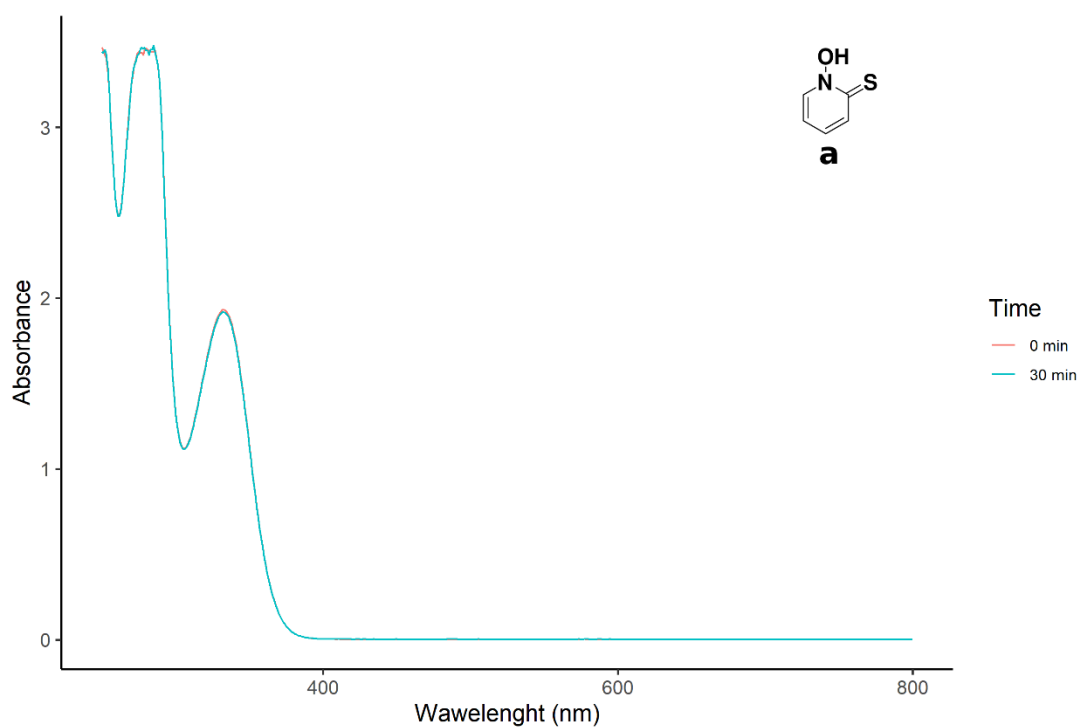


Supplementary Figure 8: ¹H NMR spectrum of 1g.

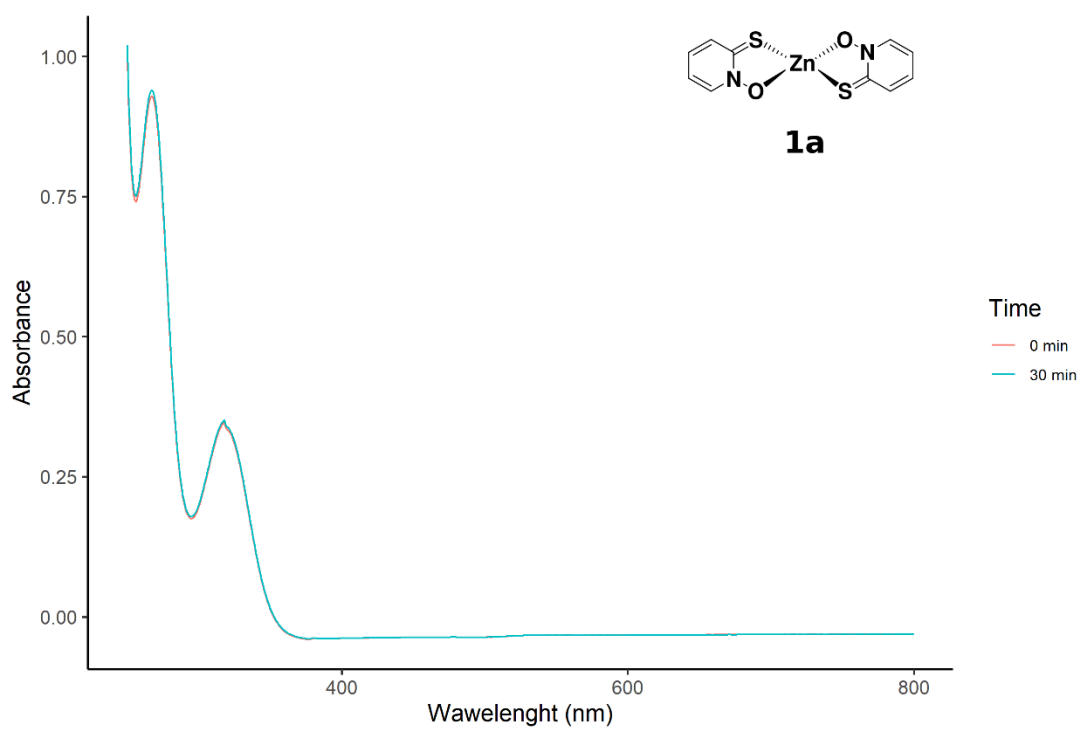


Supplementary Figure 9: ¹H NMR spectrum of 1h.

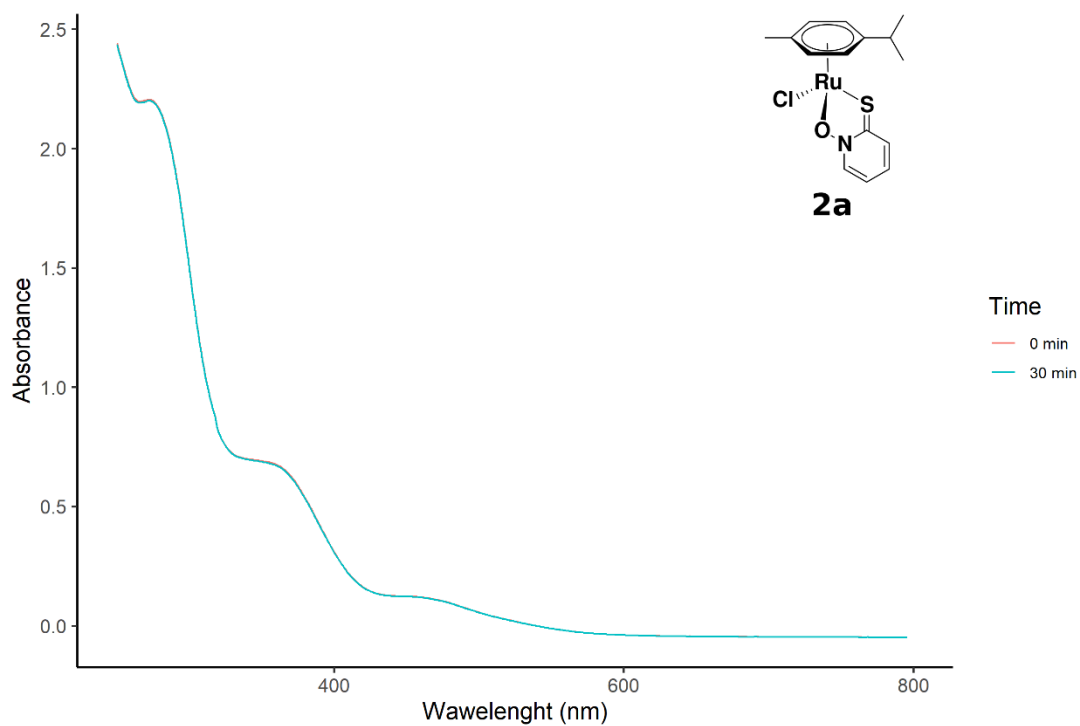
5. UV-vis and NMR stability



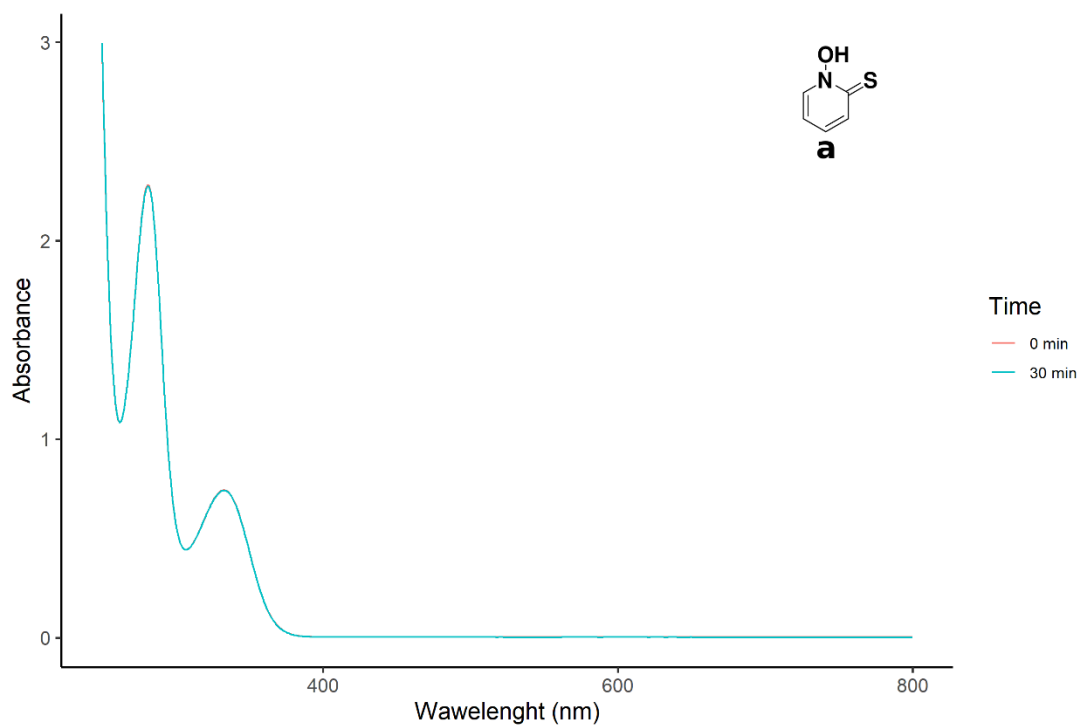
Supplementary Figure 10: UV-vis stability spectra of ligand pyrithione a in 1% DMSO/acetate buffer.



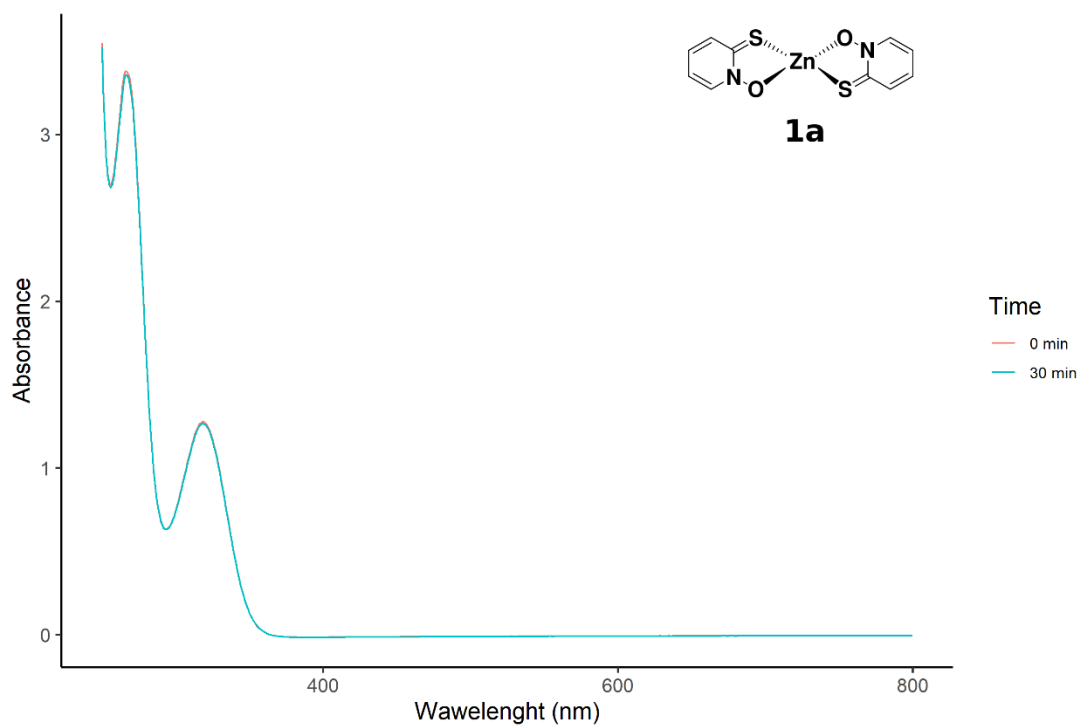
Supplementary Figure 11: UV-vis stability spectra of zinc complex 1a in 1% DMSO/acetate buffer.



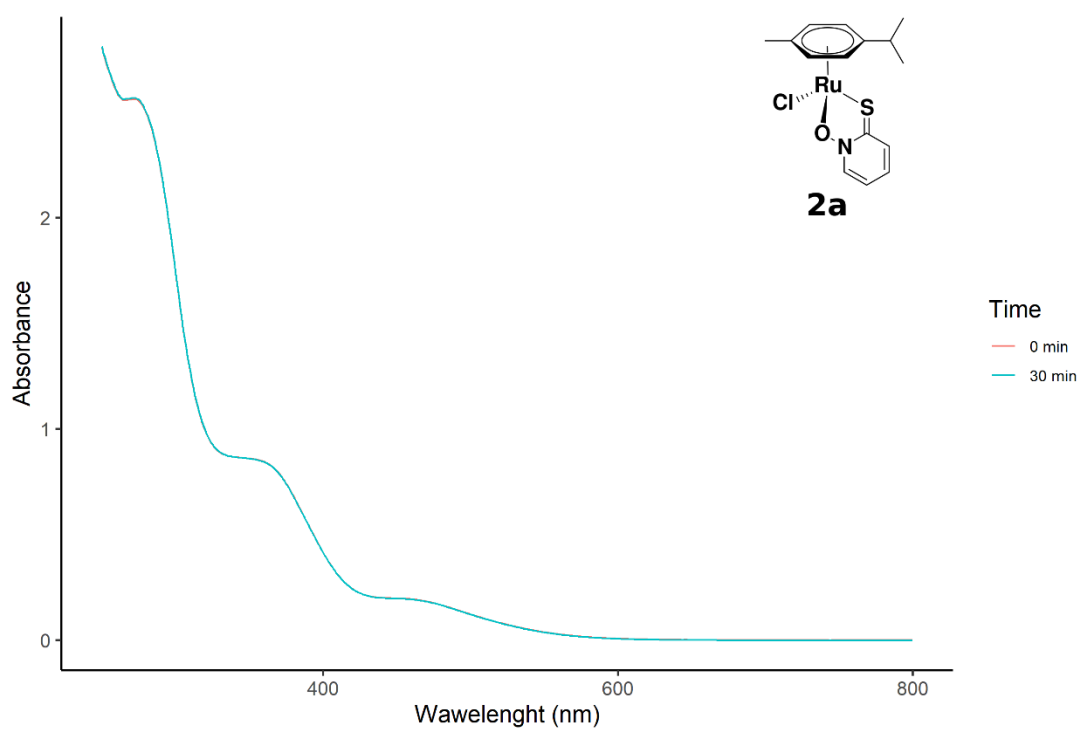
Supplementary Figure 12: UV-vis stability spectra of ruthenium complex 2a in acetate buffer.



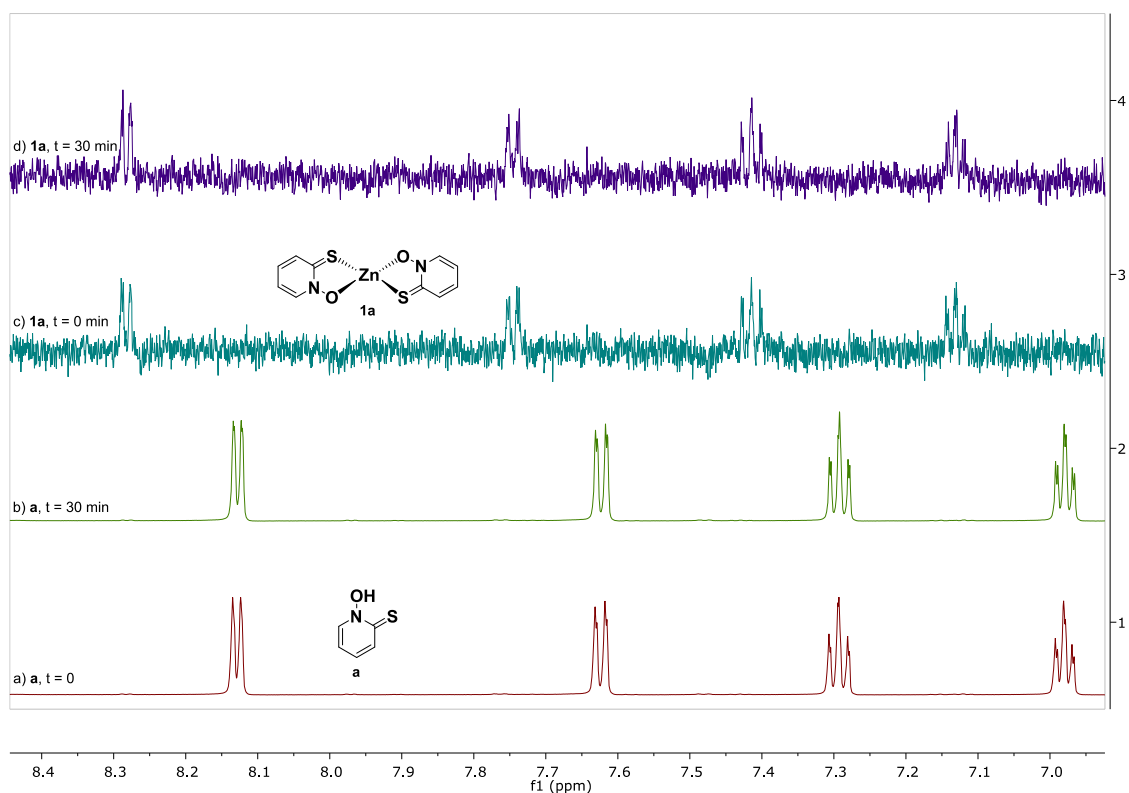
Supplementary Figure 13: UV-vis stability spectra of ligand pyriothione a in 1% DMSO/HEPES buffer.



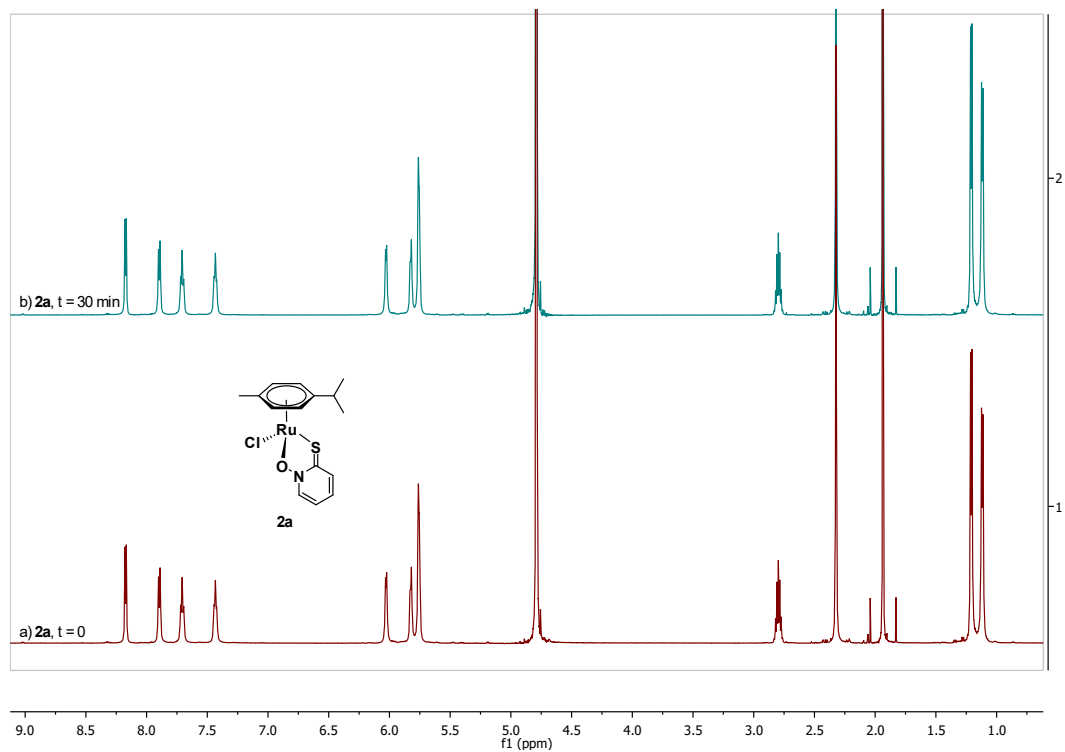
Supplementary Figure 14: UV-vis stability spectra of zinc complex 1a in 1% DMSO/HEPES buffer.



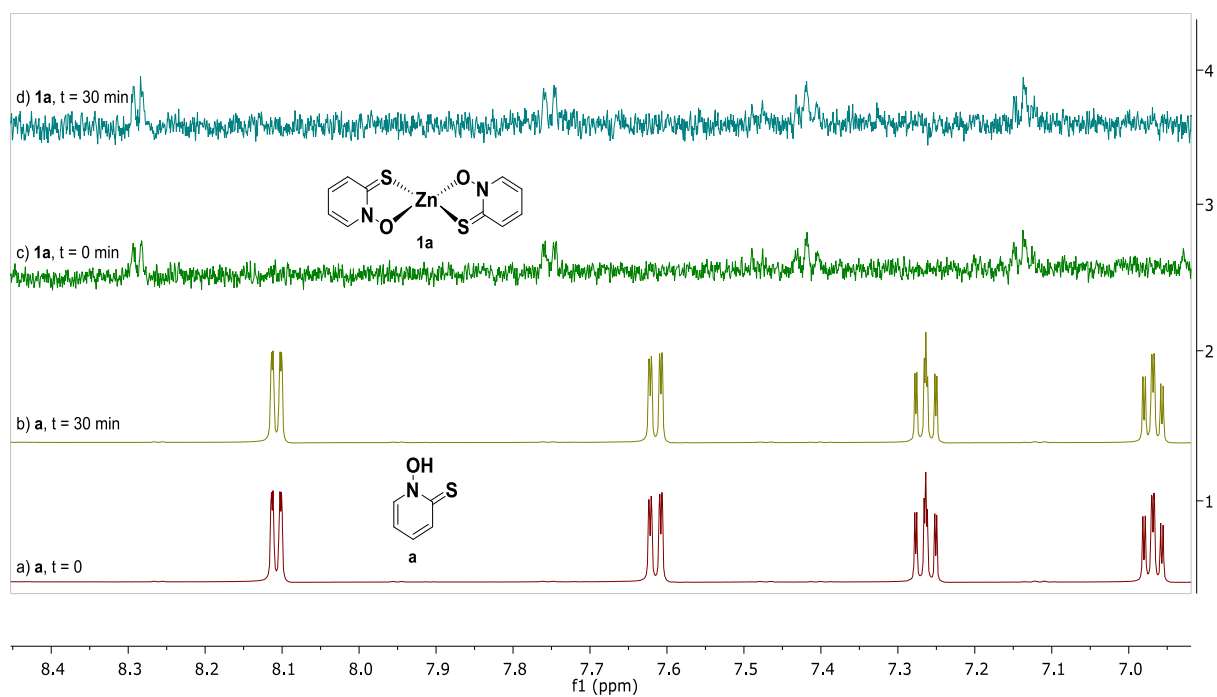
Supplementary Figure 15: UV-vis stability spectra of ruthenium complex 2a in HEPES buffer.



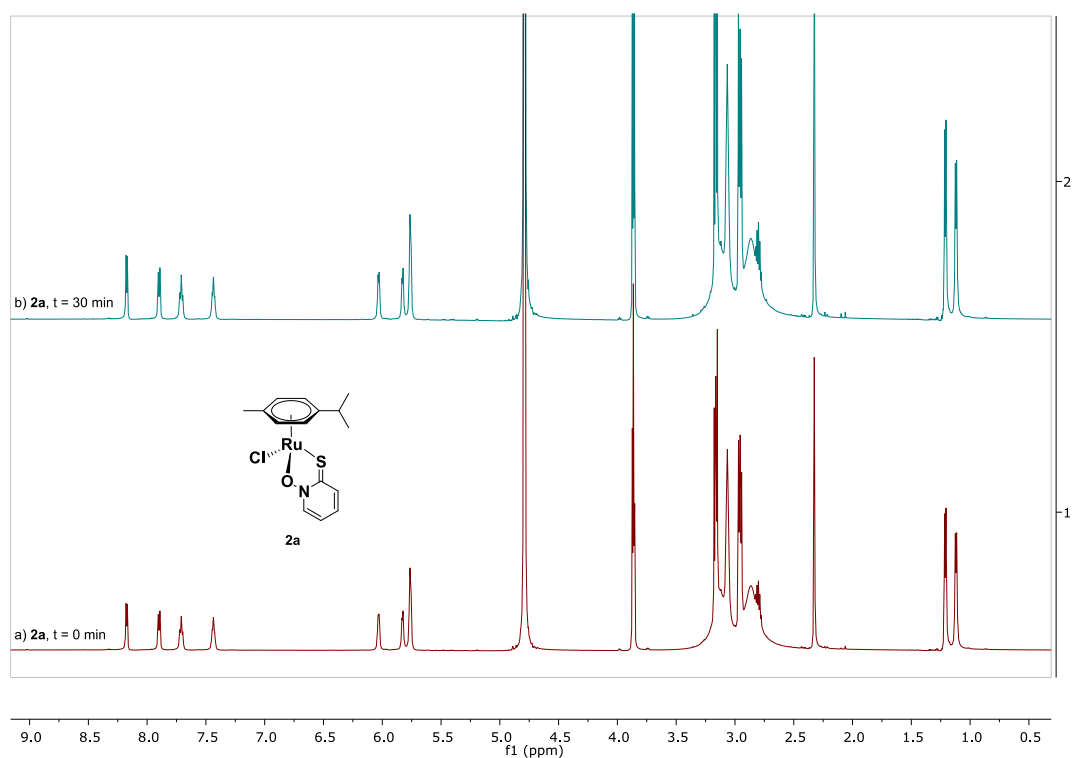
Supplementary Figure 16: ^1H NMR stability spectra of pyrithione **a (a–b) and zinc complex **1a** (c–d) in 1% $\text{DMSO-}d_6$ /acetate buffer solution prepared in D_2O recorded immediately after preparation and after 30 min.**



Supplementary Figure 17: ^1H NMR stability spectra of ruthenium complex with pyrithione **2a in acetate buffer solution prepared in D_2O recorded immediately after preparation and after 30 min.**

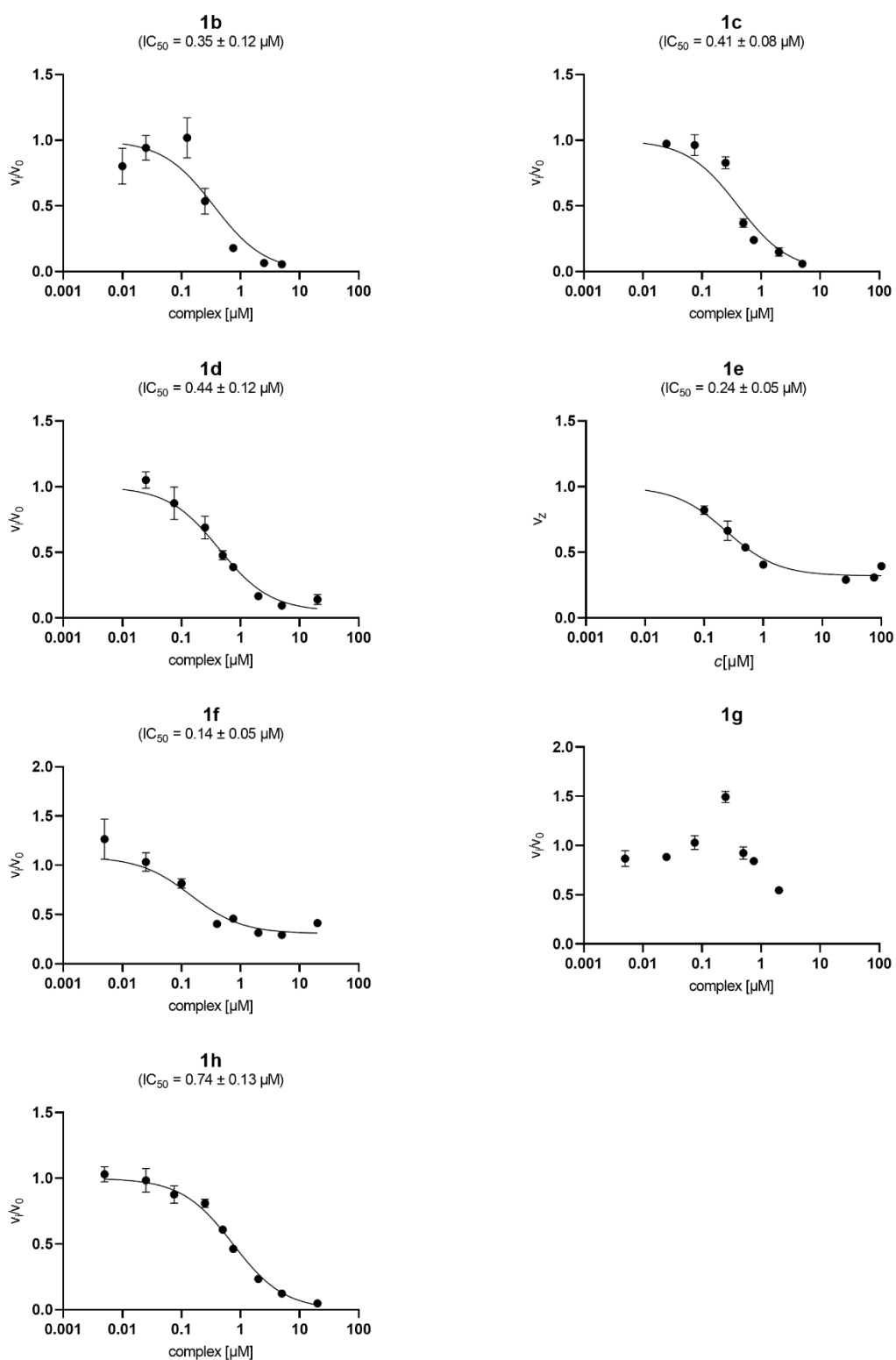


Supplementary Figure 18: ^1H NMR stability spectra of pyriothione a (a–b) and zinc complex 1a (c–d) in 1% $\text{DMSO-}d_6/\text{HEPES}$ buffer solution prepared in D_2O recorded immediately after preparation and after 30 min.

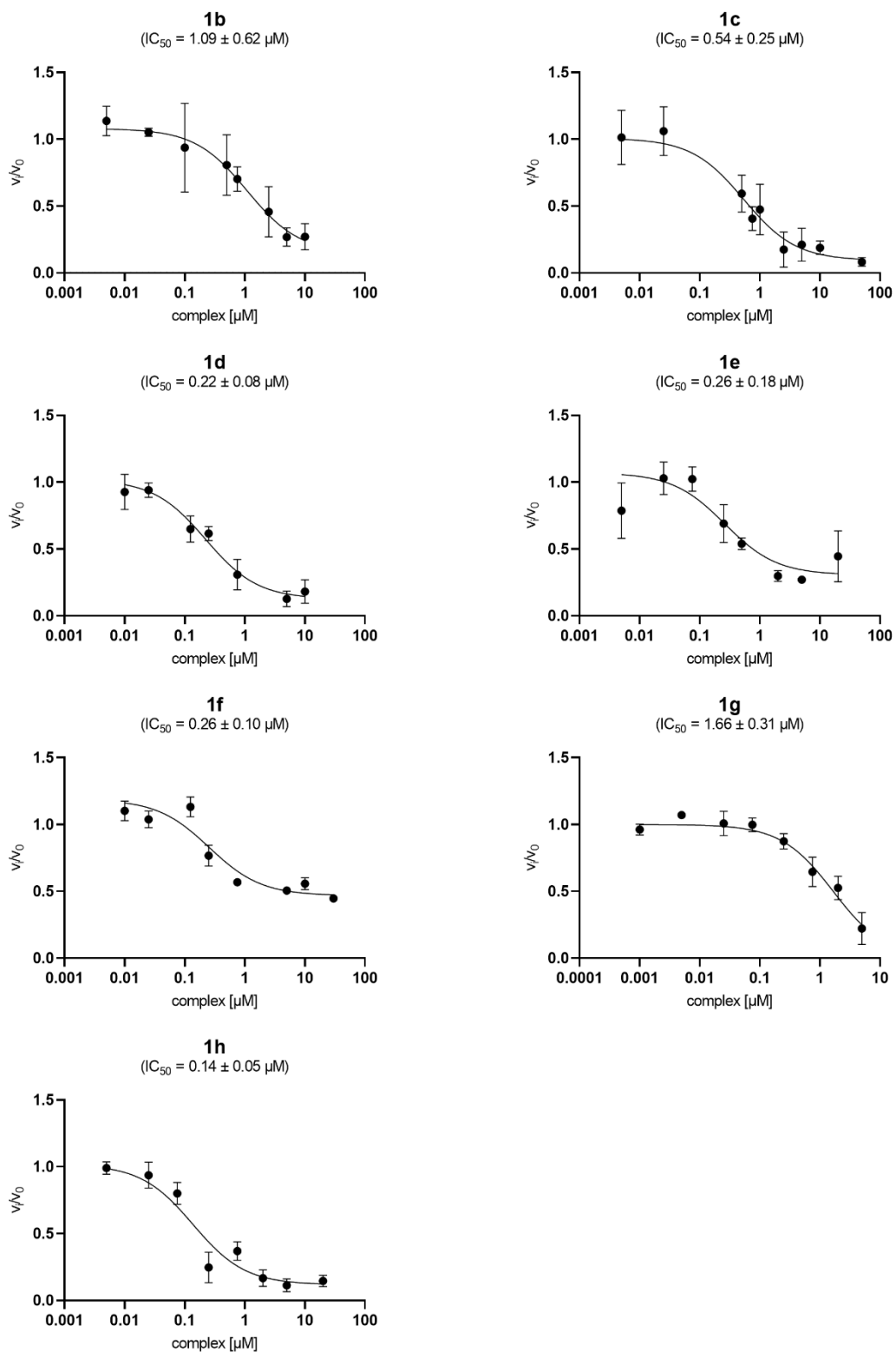


Supplementary Figure 19: ^1H NMR stability spectra of ruthenium complex with pyriothione 2a in HEPES buffer solution prepared in D_2O recorded immediately after preparation and after 30 min.

6. Enzyme assays



Supplementary Figure 20: Results of enzyme inhibition assays for cathepsin L. Data are mean \pm s.e.m. of three measurements.

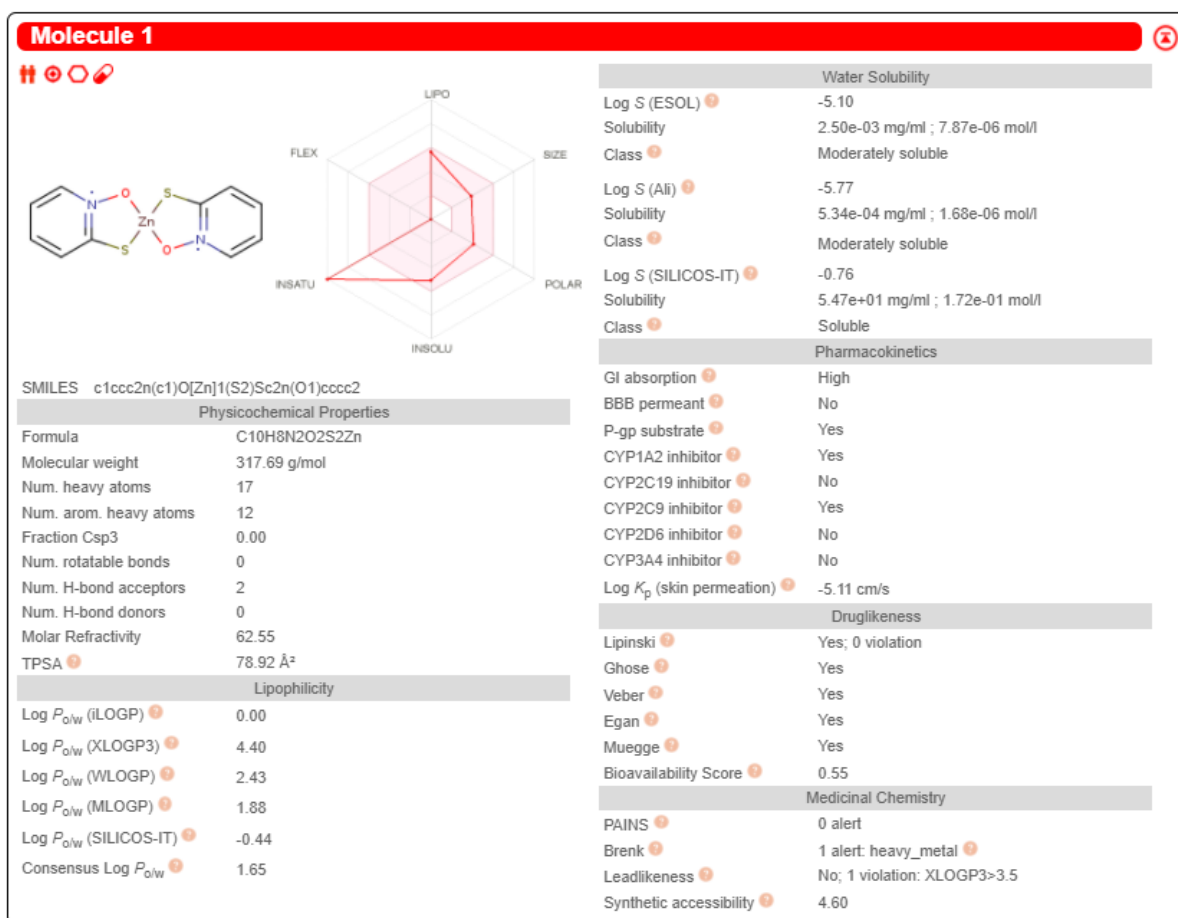


Supplementary Figure 21: Results of enzyme inhibition assays for PL^{Pro}. Data are mean \pm s.e.m. of three measurements.

Supplementary Table 3: Relative reaction rates for ligands tested on Cahtepsin L and PL^{Pro}. Data are averages of three measurements.

Ligand	v_i/v_0 at 100 μM	
	Cathepsin L	PL^{Pro}
a (Pth)	1.09	0.88
b (3MePth)	1.05	0.50
c (4MePth)	1.04	0.60
d (5MePth)	1.01	0.77
e (6MePth)	1.15	0.82
f (1iQth)	0.65	0.66
g (2Qth)	0.53	0.28
h (3OMePth)	1.17	0.60

7. Prediction data for the key parameters in drug design



Supplementary Figure 22: Evaluation of physicochemical properties, pharmacokinetics, drug-likeness and medicinal chemistry friendliness of zinc pyrithione **1a**.⁹

8. References

1. *CrysAlis PRO*; Oxford Diffraction Ltd.: Yarnton, Oxfordshire, UK, 2011.
2. Dolomanov, O. V, Bourhis, L. J., Gildea, R. J., Howard, J. A. K. & Puschmann, H. *OLEX2: a complete structure solution, refinement and analysis program. J. Appl. Crystallogr.* **42**, 339–341 (2009).
3. Sheldrick, G.M. *SHELXL2018/3*; University of Göttingen: Göttingen, Germany, 2018.
4. Macrae, C. F. *et al.* Mercury: visualization and analysis of crystal structures. *J. Appl. Cryst.* **39**, 453–457 (2006).
5. CCDC. <https://www.ccdc.cam.ac.uk/structures/>. Accessed: 1. 3. 2022.
6. Barnett, B. L., Kretschmar, H. C. & Hartman, F. A. Structural characterization of bis(*N*-oxopyridine-2-thionato)zinc(II). *Inorg. Chem.* **16**, 1834–1838 (1977).
7. Xiong, R. G., Song, B. L., You, X. Z., Mak, T. C. W. & Zhou, Z. Y. Syntheses and properties of some transition metal complexes with methyl substituted 1-hydroxy-2(1*H*)-pyridinethione and crystal structure of bis(1-hydroxy-4-methyl-2(1*H*)pyridinethionato-O,S')zinc(II). *Polyhedron* **15**, 991–996 (1996).
8. West, D. X. *et al.* Crystal structures of the cobalt(III), nickel(II), copper(II), and zinc(II) complexes of 2-thio-6-picoline *N*-oxide. *J. Chem. Crystallogr.* **28**, 853–860 (1998).
9. SwissADME. <http://www.swissadme.ch/index.php>. Accessed: 1. 3. 2022.